"negligible" turbulence for this aircraft. Here $QS = q/V_0$, where q is the root-mean-square (rms) turbulence velocity. The QS value for a given level of turbulence is almost twice as large for the cruise configuration as for the landing configuration.

Thus, from the model results shown in Figs. 3 and 4 for a B-747 aircraft, even small amounts of density stratification or atmospheric turbulence could cause the observation of an $H = 6$ limit on wake migration, and this is especially true for the cruise configuration. It is not known how often the conditions of near-zero stratification and turbulence occur. However, they may occur so infrequently that they do not normally affect aircraft operations.

Concluding Remarks

The data in Figs. 1 and 2 indicate that the choice of flow-visualization method used in an experiment can have an important influence on the interpretation of the maximum vortex lifetime and the maximum vortex migration distance. Vortices are observed to migrate farther and last longer using neutrally buoyant particles rather than using dye to visualize the vortex motion. Similarly, Figs. 3 and 4 show that the maximum, measured full-scale vortex descent distance may be influenced strongly by atmospheric conditions (which were not measured during most flight tests). Thus, the 900-ft descent distance, which is commonly thought to be the maximum migration limit for full-scale aircraft, may not, in fact, be the maximum limit.

The new, laboratory wake measurements presented here are significant in their own right; however, the authors believe these results and the implications of incorporating different visualization techniques may be of interest to researchers studying other aircraft vortex flows.

The evolution and migration of vortices is applicable to a wide class of aerospace problems. The data presented here point out the deficiencies in our current understanding of vortex motions. The evolution is even less well understood if we include ground effect, wind, and other environmental factors.

Acknowledgments

This study was supported by the Office of Naval Research under Contracts N00014-88-C-0284 and N00014-89-C-0030. The authors thank Lee E. Piper and Raminder Singh for useful discussions and their assistance in performing the experiments. Thanks also to T. Sarpkaya for useful discussions on an early draft of this Note.

References

[1]Campbell, J. F., Chambers, J. R., and Rumsey, C. L., "Observation of Airplane Flowfields by Natural Condensation Effects," *Journal of Aircraft,* Vol. 26, July 1989, pp. 593–604.

[2]Sarpkaya, T., "Trailing Vortices in Homogeneous and Density-Stratified Media," *Journal of Fluid Mechanics,* Vol. 136, Nov. 1983, pp. 85–109.

[3]Condit, P. M., and Tracy, P. W., "Results of the Boeing Company Wake Turbulence Test Program," *Aircraft Wake Turbulence and Its Detection,* edited by J. H. Olsen, A. Goldburg, and M. Rogers, Plenum, New York, 1971, pp. 473–508.

[4]Delisi, D. P., and Orlanski, I., "On the Role of Density Jumps in the Reflexion and Breaking of Internal Gravity Waves," *Journal of Fluid Mechanics,* Vol. 69, Pt. 3, 1975, pp. 445–464.

[5]Delisi, D. P., and Dunkerton, T. J., "Laboratory Observations of Gravity Wave Critical-Layer Flows," *Pure and Applied Geophysics,* Vol. 130, No. 2/3, 1989, pp. 445–461.

[6]Tomassian, J. D., "The Motion of a Vortex Pair in a Stratified Medium," Ph.D. Thesis, Univ. of California, Los Angeles, CA, 1979.

[7]Greene, G. C., "An Approximate Model of Vortex Decay in the Atmosphere," *Journal of Aircraft,* Vol. 23, July 1986, pp. 566–573.

Airfoil Design for Endurance Unmanned Air Vehicles

Richard M. Howard*
Naval Postgraduate School, Monterey, California 93943

Nomenclature

C_d = airfoil section drag coefficient
C_D = aircraft drag coefficient
C_l = airfoil section lift coefficient
C_L = aircraft lift coefficient
x = streamwise coordinate
y = transverse coordinate
α = angle of attack

Introduction

THE current classifications for unmanned air vehicles (UAVs) for military use include, among others, an endurance UAV with a mission requirement of remaining aloft for a period of days. Though many of the proposed vehicles are large (the Boeing Condor, which set two altitude records in 1989, has a 200-ft wingspan[1]), the high altitudes at which these aircraft are expected to fly place the operating flight conditions in the low Reynolds number regime. In the 1970s, when few general-aviation aircraft manufacturers were designing their own airfoils, it was not uncommon for a manufacturer to select an airfoil from the text of Abbott and von Doenhoff.[2] Sailplane competition had long before driven soaring enthusiasts to consider more highly optimized contours for low Reynolds number flight, resulting in the development of many excellent airfoils by Wortmann and Eppler. It can be expected that many advances in aerodynamics for endurance UAVs will be derived from current sailplane technology.

High-altitude long-endurance propeller-driven unmanned aircraft require not only a high C_L/C_D, but, more importantly for concerns of maximum time aloft, a high value of $C_L^{3/2}/C_D$. This dependence can be noted from the Breguet endurance equation,[3] from which it can also be noted that consideration must be given to the speeds where propeller efficiency and fuel consumption are optimal. Maximizing endurance will in actuality involve a compromise between these various factors. In any case, a high value of the endurance parameter $C_L^{3/2}/C_D$ is certainly desirable. The effect is to weight the high-lift, low-drag benefits toward the high-lift end of the flight spectrum. As noted in Ref. 4, it is not necessarily the airfoil with the lowest drag coefficient that may be optimum; a higher maximum lift coefficient allows the aircraft to have less wing area for a specified minimum airspeed, which reduces the overall wing profile drag. A tradeoff of drag for lift may prove to be worthwhile for a vehicle such as the endurance UAV, which may have very narrow design constraints. A somewhat similar approach was taken for the Voyager aircraft that circled the world without refueling—to avoid the possible loss of lift on the canard from surface contamination, drag-producing vortex generators were attached to the canard's upper surface.

The Eppler method, described in Ref. 5, was used to develop a low Reynolds number airfoil suitable for the requirements of an endurance UAV. Airfoil performance parameters

Received Dec. 1, 1989; revision received March 1, 1990; accepted for publication March 27, 1990.

*Assistant Professor, Department of Aeronautics and Astronautics. Member AIAA.

are compared to those for other airfoils being considered for, or designed for, the same requirements.

Design Requirements

Two general approaches to low-speed airfoil design have been followed recently. General and experimental aviation have made great gains in aerodynamic improvements, with an increased interest in reduced viscous drag and the design of a family of airfoils with natural laminar flow (NLF).[6] These NLF airfoils are characterized by long runs of laminar flow, with transition ramps to enforce transition before the strong pressure recovery and separation ramps near the trailing edge to prevent separation over the main recovery region at angles of attack below those approaching stall. The family of NLF airfoils is noted for low drag, gentle stall behavior, and maintaining a value of maximum lift coefficient regardless of surface contamination (though with an increased drag).

The other approach has pursued a quest for maximum lift, resulting in airfoils generally referred to as "Liebeck" airfoils.[7] The Liebeck L1003 airfoil, for example, has achieved, at a Reynolds number of 1 million, a maximum C_l/C_d of 220 and a maximum $C_l^{3/2}/C_d$ of 360. But this airfoil was not designed for practical application, as it suffers an abrupt stall behavior (due to its Stratford pressure recovery); it was designed as an exercise in high lift.

To design an airfoil for optimized endurance, it was desired to achieve the high lift characterized by Liebeck airfoils but with the gentle stall behavior of the new family of NLF airfoils. Note that a drag penalty may be incurred at low-lift coefficients, but it is desired that high-lift coefficients be achieved without further large increases in drag, resulting in improved values of the airfoil endurance parameter, as well as of C_l/C_d, at very high-lift conditions. Of course, an optimum $C_l^{3/2}/C_d$ for the airfoil does not translate directly into an optimum $C_L^{3/2}/C_D$ for the entire aircraft. The airfoil must be integrated into the design and provides only one part of the vehicle's performance.

HG(1)-1715 Airfoil

The resulting airfoil, designated the HG(1)-1715, is shown in Fig. 1, along with the velocity distribution at 8-deg angle of attack. The designation of the HG airfoil indicates its original mission and follows standard NASA practice: HG stands for hang glider, (1) for the first in the series, 17 for the design C_l of 1.7 (where C_l/C_d is a maximum), and 15 for 14.8% maximum thickness. Coordinates are available from the author. As mentioned earlier, the airfoil was designed using the Eppler method, which takes prescribed velocity-distribution characteristics and conformally maps the design-airfoil surface. The potential flow about the airfoil is solved by a panel method and is combined with an integral-boundary-layer analysis to produce lift-curve, drag-polar, and transition and separation predictions. The design Reynolds number was 1 million, representative for this class of aircraft.[8]

The displayed velocity distribution is at a C_l near the design value of 1.7. The flow over the upper surface accelerates to a run of constant pressure, then goes through a "transition ramp" and transitions to turbulent flow at about 26% chord. The flow progresses through a concave pressure recovery with an abrupt recovery near the trailing edge. The lower surface is seen to slowly accelerate all the way to the trailing edge. An important feature of the design was to maintain a favorable or neutral pressure gradient to the transition ramp region, up to the design angle of attack. Separation over the upper surface is progressive, increasing linearly from 95 to 50% chord as the angle of attack increases from 10 to 16 deg. In the Eppler method described in Ref. 5, the boundary-layer characteristics are calculated from the potential-flow pressure distribution; no iteration between the boundary-layer displacement thickness and the pressure distribution is performed. The computer code cannot solve through a separated region; viscous corrections are applied to take the boundary-layer separation into account. Correlation between analytical and experimental results through stall using this method have been good; see Ref. 9 for an example.

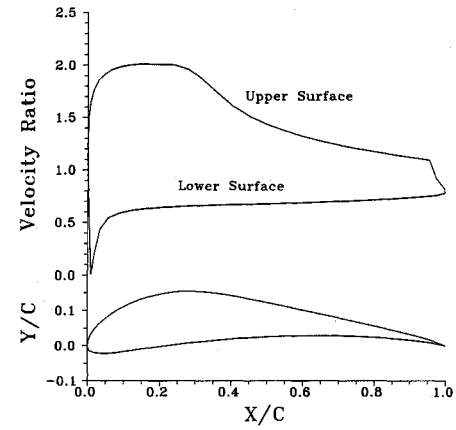

Fig. 1 HG(1)-1715 airfoil and velocity distribution at 8 deg angle of attack.

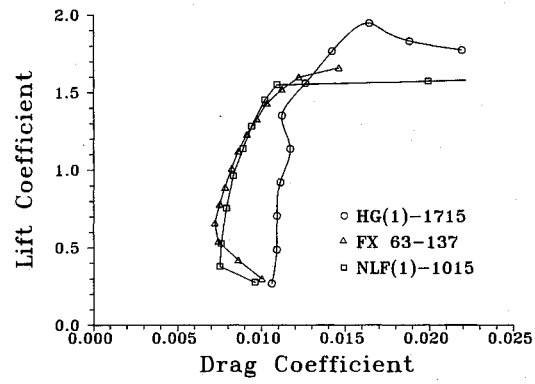

Fig. 2 Drag polars for endurance UAV airfoils.

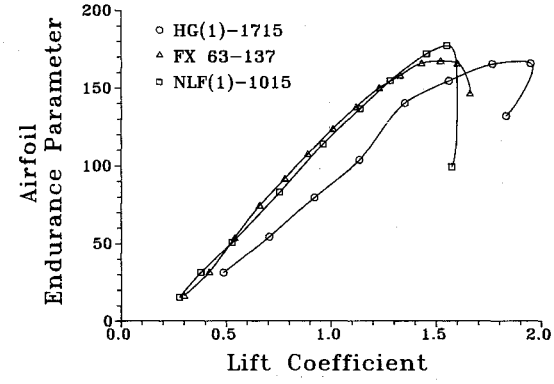

Fig. 3 Endurance parameter for UAV airfoils.

Figure 2 shows the drag polar for the HG(1)-1715 airfoil, along with those for the FX 63-137 and the NLF(1)-1015. The data for the Wortmann airfoil are experimental data taken from Refs. 10 and 11; the data for the NLF airfoil are taken from Ref. 4. It should be noted that the Wortmann and NLF airfoil data are shown for a Reynolds number of 0.7 million; those for the HG airfoil are for Re = 1 million. A small bias may be introduced, due to the fact that aerodynamic characteristics usually improve with Reynolds number, but this is not always true. For example, the lift for a given angle of attack actually decreases for the Wortmann airfoil as the Reynolds number is increased from 0.5 to 0.7 million.

First to be noted is the drag penalty over the lift range from C_l = 0.3 to 1.5 for the HG airfoil. The transition location on the upper surface is fairly constant (moving from 32 to 21%

arclength) for the complete angle-of-attack range from −6 to 14 deg; a long run of laminar flow is not present. But for a C_l above 1.5, the drag increase for the other two airfoils is significant, whereas the HG airfoil continues with moderately increasing drag up to a maximum lift coefficient of 1.95. Whereas the NLF airfoil reaches its $C_{l\max}$ at $C_d = 0.025$, the HG airfoil reaches its $C_{l\max}$ at a C_d of 0.016.

Plots of the airfoil endurance parameter, $C_l^{3/2}/C_d$, for the three airfoils are shown in Fig. 3. The Wortmann and HG airfoils reach identical maximum values of about 165, whereas the NLF airfoil reaches a slightly higher value of 175. But note that the other two airfoils peak at $C_l = 1.55$, whereas the HG airfoil peaks at $C_l = 1.85$. Therefore, an endurance UAV with the HG airfoil would be able to remain aloft comparably to others with FX or NLF airfoils but at a significantly higher lift coefficient and therefore lower speed (or identical speed with less wing area). Within the limits of the assumptions of the Breguet endurance equation, where the engine/propeller characteristics are not being treated, a loitering ability may be maximized using the airfoil with the higher lift coefficient at the same value of endurance parameter.

A long run of laminar flow is not necessarily an important requirement for all aircraft designs. To maximize an endurance capability, a tradeoff of increased drag at low-lift values for reduced drag at very high-lift conditions may be beneficial.

References

[1]"Tech News," *Mechanical Engineering*, Vol. 111, No. 9, Sept. 1989, p. 89.

[2]Abbott, I. H., and von Doenhoff, A. E., *Theory of Wing Sections,* McGraw-Hill, New York, 1949.

[3]Anderson, J. D., Jr., *Introduction to Flight,* 3rd ed., McGraw-Hill, New York, 1989, p. 308.

[4]Maughmer, M. D., and Somers, D. M., "An Airfoil Designed for a High-Altitude Long Endurance Remotely Piloted Vehicle," AIAA Paper 87-2554, Aug. 1987.

[5]Eppler, R., and Somers, D. M., "A Computer Program for the Design and Analysis of Low-Speed Airfoils," NASA TM 80210, 1980.

[6]Somers, D. M., "Design and Experimental Results for a Flapped Natural-Laminar-Flow Airfoil for General Aviation Applications," NASA TP 1865, June 1981.

[7]Liebeck, R. H., "On the Design of Subsonic Airfoils for High Lift," Douglas Paper 6463, Douglas Aircraft Co., Long Beach, CA, July 1976.

[8]Henderson, C., and McQuillen, E., "High Altitude, Long Endurance RPV Design Technology Study," Naval Air Development Center, Warmister, PA, Rept. NADC-85060-60, March 1985, pp. 43.

[9]Somers, D. M., "Design and Experimental Results for a Natural-Laminar-Flow Airfoil for General Aviation Applications," NASA TP 1861, June 1981, p. 88.

[10]Miley, S. J., *A Catalog of Low Reynolds Number Airfoil Data for Wind Turbine Applications,* Dept. of Aerospace Engineering, Texas A&M Univ., College Station, TX, Feb. 1982, pp. 19–23.

[11]Althaus, D., and Wortmann, F. X., *Stuttgarter Profilkatalog I,* Friedr. Vieweg und Sohn, Braunschweig, FRG, 1981, p. 79.

Constant Swirl Angle Inlet Guide Vanes

Richard M. Andres*

Parks College, St. Louis University, Cahokia, Illinois 62206

Nomenclature

m	= velocity profile exponent − defined in text
n	= polytropic exponent
RH,RT	= hub and tip radius, respectively
r	= radial coordinate
U	= upstream and uniform axial velocity
u,v_r,v_θ	= axial, radial, and tangential velocity components, respectively
x,y	= dummy variables
γ	= ratio of specific heats
μ	= defined in text; $\mu = 1$ for isentropic flow
ω	= angular velocity of a compressor rotor

Subscripts

1, 2	= upstream and downstream, respectively

Received Oct. 27, 1989; revision received March 5, 1990.

*Professor of Aerospace Engineering. Member AIAA.

Introduction

WIND-TUNNEL compressors can benefit from the use of variable inlet guide vanes. This is especially true if the drive is constant speed and/or the compressor or fan is fixed pitch. When inlet guide vanes are used, it is desirable to make at least some part of the vane system structurally rigid, usually connecting a nose fairing to the drive section ducting. The trailing-edge sections of the support vanes can be made movable with a simple flap arrangement. The inlet guide vane system can therefore consist of a simple untwisted symmetric airfoil section with plain flaps at the aft 40 or 50% of the chord. NASA Ames is considering such a geometry for the modification of existing wind tunnels. If the chord and thickness of the airfoils are increased in proportion to the radial station, the vanes will have a constant solidity. Neglecting secondary effects, such as the radially increasing vane chord Reynolds number, a constant turning angle (swirl angle) of the flow should result. A solution for the axial and tangential velocity distributions is presented. The analysis is restricted to the case of a frictionless and incompressible flow with a uniform and axial velocity upstream of the inlet guide vane system.

Analysis

The energy equation may be combined with the radial equilibrium equations upstream and downstream of a rotor (or stator) to yield the equation[1]

$$u_2\frac{du_2}{dr_2} - u_1\frac{du_1}{dr_1} = (\mu-1)\left[\frac{v_{\theta 1}^2}{r_1} - \frac{v_{\theta 2}^2}{r_2}\right]$$

$$+\left[\frac{v_{\theta 1}}{r_1} - \omega\right]\frac{d(v_{\theta 1}r_1)}{dr_1} - \left[\frac{v_{\theta 2}}{r_2} - \omega\right]\frac{d(v_{\theta 2}r_2)}{dr_2} \qquad (1)$$

where μ is given by $\mu = (\gamma/n)[(n-1)/(\gamma-1)]$, and $\mu = 1$ for isentropic flow. For Eq. (1), the radial velocity contribution has been neglected according to

$$v_r^2 \ll u^2 + v_\theta^2$$

For the inlet guide vane, $\omega = 0$. The inlet velocity is taken as axial and uniform ($u = U$). If the vane loss is assumed small, $\mu = 1$ (isentropic), the throughflow equation reduces to

$$u_2\frac{du_2}{dr_2} = \frac{v_{\theta 2}}{r_2}\frac{d(v_{\theta 2}r_2)}{dr_2} \qquad (2)$$

Inlet guide vanes with a constant solidity and constant flap chord to total chord ratio should produce a nearly uniform